Modelling of a CPV-T Collector for Combined Heat and Power Generation

Chandan Pandey[1], Mingyang Wu[1], Hasan Yildizhan[1,2], Ivan P. Acosta-Pazmiño[3], C.I. Rivera-Solorio[3], M. Gijon-Rivera[4], Rafael A. García-Ramos[3] and Christos N. Markides[1*]

[1] Clean Energy Processes Laboratory, Department of Chemical Engineering, Imperial College London, London (United Kingdom)

[2] Department of Energy Systems Engineering, Adana Alparslan Türkeş Science and Technology University, Adana 46278, Turkey

[3] Tecnologico de Monterrey, Escuela de Ingeniería y Ciencias, Ave. Eugenio Garza Sada 2501, Monterrey, (Mexico)

[4] Tecnologico de Monterrey, Escuela de Ingeniería y Ciencias, Vía Atlixcáyotl 5718, Puebla, 72453, Puebla, (Mexico)

***Corresponding author: c.markides@imperial.ac.uk**

Abstract

In this work, a coupled optical, electrical and thermal model of a concentrated photovoltaic-thermal (CPV-T) collector with a geometrical concentration ratio of 11 is developed. To estimate the accuracy of the coupled model, this is first validated against data of known collectors in the existing literature. Results show that the model can predict the optical and thermal performance of these collectors with a deviation under 8%. The model is then used to predict the performance of a new collector design. Simulation results reveal that the collector achieves a thermal efficiency of 68% and an electrical efficiency of 14% at a direct normal irradiance of 1000 W/m^2, an ambient temperature of 25 °C, an inlet water temperature of 25 °C and a mass flowrate of 0.01 kg/s. The characteristic thermal and electrical efficiency curves of the collector are also generated. Based on this CPV-T collector design, a prototype is being constructed and tests are being performed in Mexico.

Keywords: Cogeneration; concentrated solar; combined heat and power; hybrid PV-thermal; solar energy

1. Introduction

The simultaneous production of electricity and heat allows for a more efficient solar energy utilization. In particular, concentrated photovoltaic-thermal (CPV-T) collectors can play a significant role in low-carbon energy systems thank to their ability to provide a high-grade thermal energy (>70 °C) (Acosta-Pazmiño et al., 2022). Nevertheless, CPV-T technologies also present certain technical challenges such as a more complex optical design, thermal and electrical management, material selection and durability, safety and reliability along with economic feasibility (Madurai Elavarasan et al., 2022). Addressing these challenges through research, development and innovation is crucial for advancing CPV-T technology, which has led to various numerical and experimental investigations in pursuit of advancements in this technology.

A parabolic trough-based CPV-T collector was developed and studied by Cabral et al. (2021) who reported thermal and electrical efficiencies of 58% and 8%. Karathanassis et al. (2017) designed, developed and tested a CPV-T collector with a rectangular absorber. Their experimental results showed that the collector achieved electrical and thermal efficiencies of 8% and 44%, respectively. Deymi-Dashtebayaz et al. (2022) studied the influence of nanofluids as heat transfer fluids on the electrical and thermal performance of a CPV-T collector, while Demircan et al. (2023) developed a finite volume-based numerical model to estimate the thermal and electrical performance of a CPV-T collector. The model predicted a PV cell temperature of roughly 110 °C at an inlet temperature of the heat transfer fluid (HTF) of 50 °C.

A review of the literature on CPV-T collectors reveals that significant work, both numerical and experimental, has already been done on CPV-T collectors. However, to the best knowledge of the authors, none of the models

© 2023. The Authors. Published by International Solar Energy Society
Selection and/or peer review under responsibility of Scientific Committee
10.18086/swc.2023.03.10 Available at http://proceedings.ises.org

presented in the literature feature coupled optical and thermal models in a single design tool. Chandan et al. (2022) used Zemax to estimate the optical flux reaching the absorber of an LCPV-T module, which was then used as input to a CFD model. Similarly, Parthiban et al. (2022) and Barthwal & Rakshit (2022) used the optical software tools Solatrace and Tracepro, respectively, to estimate the optical flux for use in a CFD model. This study aims to develop a coupled optical electrical and thermal model for a CPV-T collector using single modelling tool. The single modelling tool will reduce the errors in the estimation of the performance of the collectors. Results from the developed model are presented in this work.

2. Methodology

2.1. Model description

The main components of the CPV-T collector studied here are an optical concentrator, PV cells and a HTF, as shown in Fig. 1. Since the aim of the present study is to retrofit commercialized parabolic trough-based solar thermal collectors with PV cells, a commercially available parabolic trough with a geometrical concentration ratio of 11 was selected for this work. The aperture width of the collector is 1.1 m and the length of the collector is 3 m. The hybrid receiver is a triangular channel constructed from an aluminum sheet of thickness 0.005 m and an illuminated area of 0.3 m^2. Solar cells are attached on two faces of the triangular channel which are illuminated area of the channel. Cells are attached in such a way that they are thermally in contact with the channel, but electrically insulated. To cool the solar cells and extract useful heat, water is used as the HTF. A cover glass of outer diameter 0.07 m and thickness 0.002 m is used to cover the receiver and trap the long wavelength radiation.

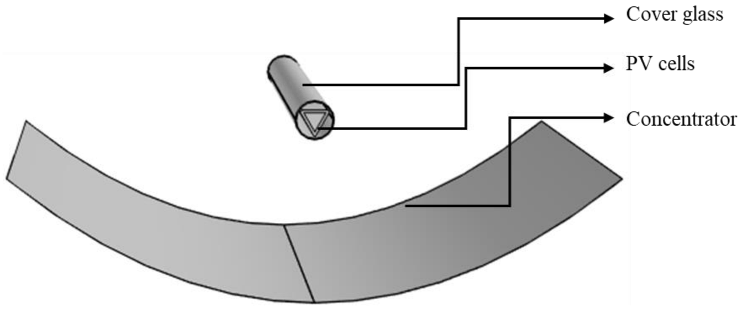

Fig. 1: Simple schematic of the CPV-T collector design investigated in the present work

2.2. Optical and thermal models

An optical model of the concentrator was developed using the COMSOL ray tracing module, allowing us to estimate the flux distribution over the cells. The ray tracing is based on the law of reflection where the angle of incidence is equal to the angle of reflection, following the governing equation given as (Chandan et al., 2022):

$$r_{\mathrm{ref}} = r_{\mathrm{inc}} - 2(n.r_{\mathrm{inc}})n \quad \text{(eq.1)}$$

where r_{ref} is the reflected ray and r_{inc} is the incident ray.

In the optical model, it was assumed that the reflectivity of the mirror is 90 % (Chandan et al., 2021) and that the transmissivity of the cover glass is 90 %. Further, the absorptivity of the solar cells was assumed to be 88 % (Chandan et al., 2021) in this study.

A 3-D CFD model was developed to estimate the thermal performance of the CPV-T collector. For the estimation of the thermal performance, it is important to couple the optical and thermal models. By implementing ray heating in the model, the flux obtained from the optical model directly becomes the incident flux on the cells. Of the total flux incident on the cells, a part of it is converted to electrical energy and the rest heats the solar cells. Therefore, it is assumed that cells act as a heat-generating source. The heat generated in the solar cells is then transferred to the triangular receiver in bottom direction by conduction which was subsequently dissipated to the cooling fluid via convection. The cells also lose heat over their top surfaces via natural convection and radiation to the surroundings. The convection loss between the solar cells and the cover glass are suppressed by maintaining a vacuum between them. Surface-to-surface radiation between the solar cell and the cover glass and cover glass and sky was considered in this study. On the top surface of the cover glass, convection heat transfer was also considered. The fluid flow inside the triangular channel was assumed to be laminar, as Reynolds number was estimated to be 1100.

With these imposed boundary conditions on the geometry of the collector, the geometrical model was discretised into small elements also referred as mesh. For each element of the discretised geometrical model, mass, momentum and energy balance equations were solved numerically. The mass, momentum and energy balance equations are (Herrando et al., 2019):

$$\rho_\mathrm{f} \nabla \cdot v_\mathrm{f} = 0 \qquad \text{(eq.2)}$$

$$\rho_\mathrm{f} v_\mathrm{f} \nabla \cdot v_\mathrm{f} = -\nabla P + \mu \nabla^2 v_f + \rho_\mathrm{f} \mathrm{g} \qquad \text{(eq.3)}$$

$$\rho_\mathrm{f} c_\mathrm{p} v_\mathrm{f} \nabla \cdot T_\mathrm{f} = \nabla \cdot (k_\mathrm{f} \nabla T_\mathrm{f}) \qquad \text{(eq.4)}$$

where P is the fluid pressure, μ the dynamic viscosity, g the acceleration due to gravity, T_f the fluid temperature, k_f the thermal conductivity of the fluid, v_f the velocity of the fluid, c_p is specific heat capacity of water and ρ_f the density of the fluid.

2.3. Electrical model

The electrical efficiency of solar cells decreases linearly with the cell temperature. To predict the electrical performance of the cells, the cell temperature was estimated by the CFD model which was then used to estimate the electrical efficiency (Huang et al., 2021; Huang & Markides, 2021; Liang et al., 2022):

$$\eta_\mathrm{PV} = \eta_0 (1 - \beta (T_\mathrm{cell} - 298\ \mathrm{K})) \qquad \text{(eq. 5)}$$

where η_0 is the base efficiency of the cell at standard test conditions (1000 W/m^2, 298 K, AM1.5G spectrum), β the power temperature coefficient, and η_pv the efficiency of the cells at an operating temperature of T_cell.

2.4. Thermal and electrical performance

The thermal efficiency of the collector is estimated by using the equation below:

$$\eta_\mathrm{th} = \frac{\dot{m}.c_\mathrm{p}.(T_\mathrm{fo} - T_\mathrm{fi})}{I.A_\mathrm{ap}} \qquad \text{(eq. 6)}$$

where η_th is the thermal efficiency of the collector, $\dot{m}$ the mass flowrate inside the collector, T_fo the outlet water temperature from the collector, T_fi the inlet water temperature to the collector, I the incident solar radiation, and A_ap the aperture of the concentrator.

The reduced temperature of the collector is given as:

$$T_\mathrm{r} = \frac{\left(\frac{T_\mathrm{fo} + T_\mathrm{fi}}{2}\right) - T_\mathrm{amb}}{I} \qquad \text{(eq. 7)}$$

where T_r is the reduced temperature of the collector, and T_amb the ambient temperature. The SI unit of reduced temperature is K.m^2/W.

3. Results and discussion

3.1. Validation of the optical model

The optical model was first validated against the simulation results presented by Hou et al. (2023). For the optical simulation, a parabolic trough concentrator of geometrical concentration ratio of 16.67 as described in the reference was created using COMSOL. 0.5 million rays were allowed to fall on the concentrator which was collected by a flat absorber of width 60 mm. The reflectivity of the concentrator was set to 90% and the absorptivity of the absorber was set to 10%. The simulation considered the Sun as a finite source with a cone angle of 4.65 mRad. The simulation also considered the limb darkening effect to ensure simulation captures actual conditions when tested in outdoor conditions. The result of the optical simulation is shown in the Fig. **2**. The result shows a fairly accurate match between the simulation results of Hou et al. (2023) and the developed optical model in COMSOL with root mean square error under 10%.

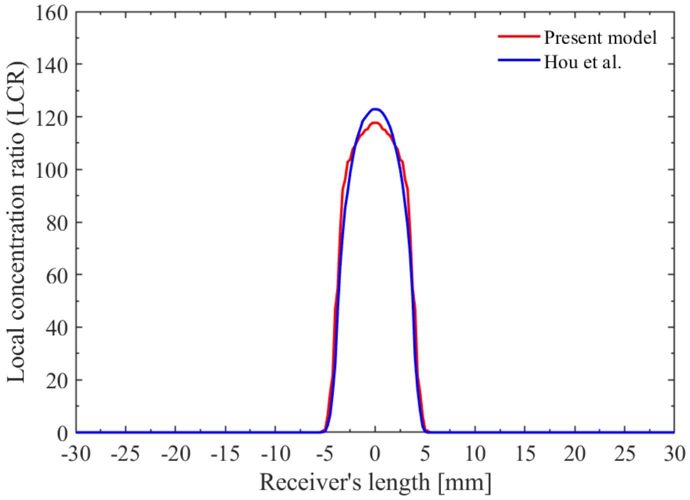

Fig. 2: Comparison of local flux distribution on the absorber

3.2. Thermal model validation

To validate the methodology of coupling the optical model with that of CFD model, work presented by Yousef et al. (2016) was selected. For this, a compound parabolic concentrator (CPC) of geometric concentration ratio 2.66, truncated to 2.4, was selected based on the literature. A PV module of dimension 0.3 m by 0.245 m was placed at the base of the CPC. Underneath the solar cell, a heat exchanger was employed. The heat exchanger was insulated from the back to reduce heat losses. Parameters such as the inlet water temperature, wind speed, insolation and ambient temperature were given as inputs to the model. The optical simulation was used to first calculate the radiation flux reaching the cells as shown in Fig. 3(b). The radiation flux was then coupled to the heat transfer model by ray heating to estimate the cell temperature, outlet water temperature and so on. The temperature distribution profile on the solar cell in shown in Fig. 3(c). The average temperature of the solar cell at different time of the day is shown in Fig. 3(a).

A comparison of results concerning the average cell temperature of the collector are shown in Fig. 3. We observe a good match between the average cell temperature predicted by the model and the experimental results of Yousef et al. (2016) with a root mean square (rms) error under 8%.

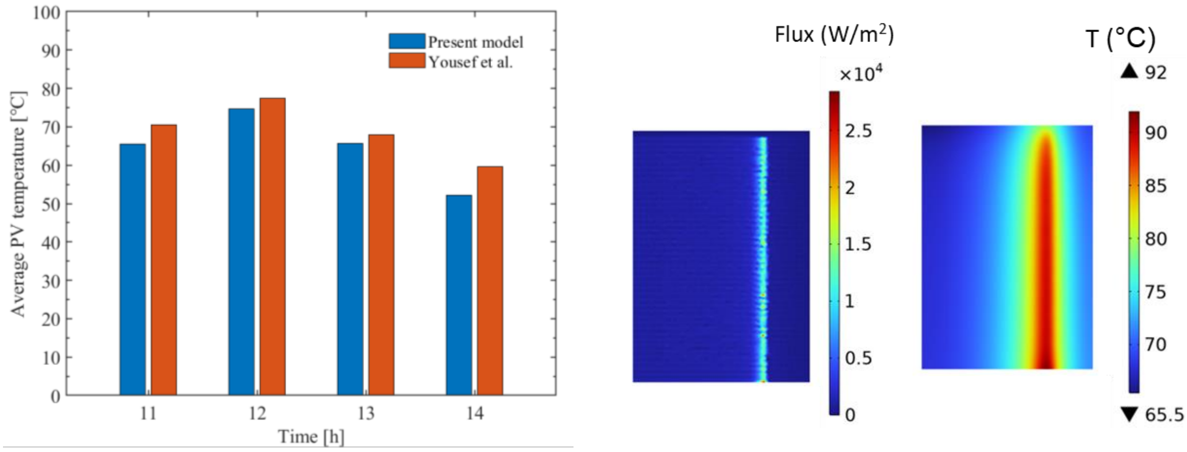

(a) **(b)** **(c)**

Fig. 3: (a) Comparison of average PV temperature, (b) local flux distribution at 12 pm, and (c) local temperature distribution on the solar cell at 12 pm.

3.3. Optical performance of the CPV-T collector

For the ray tracing of the CPV-T collector, a similar methodology as stated in Section 3.1 was followed. The number of rays falling on the absorber was set to 1 million and the reflectivity of the mirror was set to 90%. The model also included the sun as a finite source suspending a conical disc angle of 4.65 mRad. The total incidence power on the mirror was found to be 3300 W and the total power reaching the absorber was 2550 W. The loss in power was mainly due to transmission losses from the cover glass and reflection losses from the mirror. The overall optical efficiency of the collector was 77%. The raytracing of the CPV-T collector is shown in Fig. 4(a), and the flux distribution on the absorber is shown in Fig. 4(b) whereas the average flux distribution on the absorber is shown in Fig. 4(c). Figure 4(c) shows the average distribution of flux on the triangular absorber when it is unfolded. The actual flux distribution on the CPV-T collector developed at test site in Mexico is shown in Fig. 4(d). The collector developed at Mexico is of same geometry as described in the section 2.1.

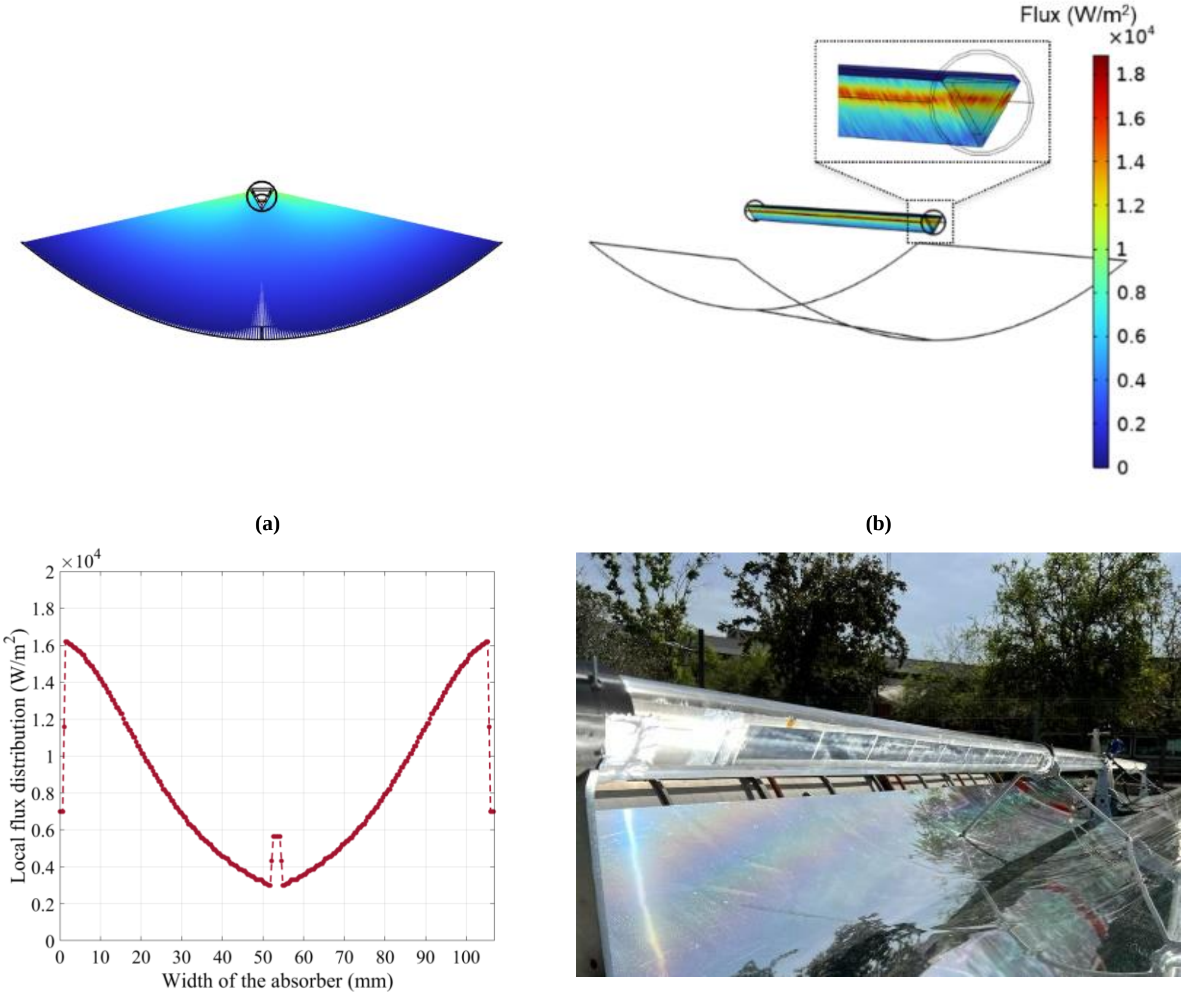

(c) **(d)**

Fig. 4: (a) Ray-tracing simulation for the collector, (b) and (c) simulation results for flux distribution on the PV cells, and (d) actual flux distribution on the test setup in Mexico

3.4. Thermal and electrical performance of the CPV-T collector

To estimate the thermal performance of the collector, the optical simulation results obtained from COMSOL were used as inputs to the thermal model. Specifically, the COMSOL optical model stores the radiation (optical) flux received on the absorber in an accumulator using a variable (*rpb*), which is then used as an input heat flux on the boundary of the receiver for the thermal model. Thus, the exact optical flux profile obtained from the optical simulation was used as input to the model to estimate the thermal performance of the collector. Furthermore, using an incident solar flux of 1000 W/m^2 at an ambient temperature of 25 °C, an inlet water temperature of 25 °C and an inlet velocity of 0.015 m/s (which is the design condition of the parabolic tough collector considered here), results show that the CPV-T collector can deliver hot water at a temperature of 77 °C, a thermal efficiency of 68%, and an electrical efficiency of 14%. The temperature distribution plot of the CPV-T collector is shown in Figure 5.

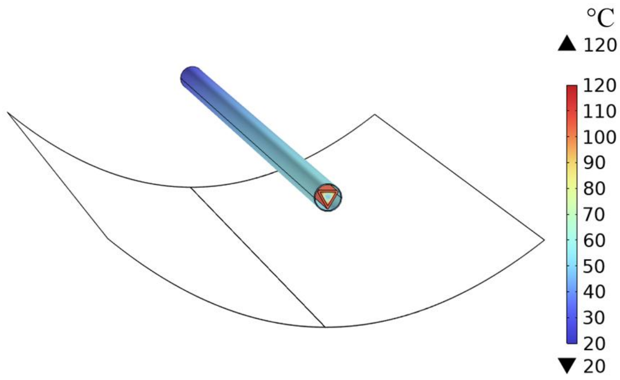

Fig. 5: Temperature distribution over the PV cells for conditions of 1000 W/m², ambient temperature of 25 °C and inlet water temperature of 25 °C and mass flowrate of 0.01 kg/s

Thereafter, characteristic thermal and electrical efficiency curves of the CPV-T collector were plotted as a function of reduced temperature, as shown in Figure 6. For this study, the characteristic curve of the CPV-T collector is plotted by fixing the mass flowrate to be 0.01 kg/s (i.e., inlet velocity of 0.015 m/s) and varying the inlet water temperature in steps of 4 °C. Single characteristic thermal and electrical efficiency plots as a function of reduced temperature within a reasonable range of operating conditions are sufficient to demonstrate the thermal and electrical performance of the collector for different operating condition such as variation of mass flowrate, irradiance, inlet water temperature and ambient temperature. In the present case, the maximum thermal efficiency of the collector when the average temperature of the receiver is close to ambient temperature is observed to be 69%. This essentially means that the collector can achieve maximum thermal efficiency of 69%, electrical efficiency of 16% and rest (15%) are the optical losses from the collector. The simulations are performed for a maximum outlet temperature of 100 °C as operating the collector above 100 °C results in two phase flow which can be taken up in another study. The characteristic thermal and electrical efficiency equations are given below. Equations 8 and 9 are obtained by fitting a polynomial of second order for thermal efficiency and first order for electrical efficiency, respectively. The temperature distribution plot for different inlet water temperature is shown in Fig. 7.

$$\eta_{\mathrm{th}} = -78.2.T_r^2 - 26.4.T_{\mathrm{r}} + 69 \quad \text{(eq. 8)}$$

$$\eta_{\mathrm{el}} = -81.5.T_{\mathrm{r}} + 16.2 \quad \text{(eq. 9)}$$

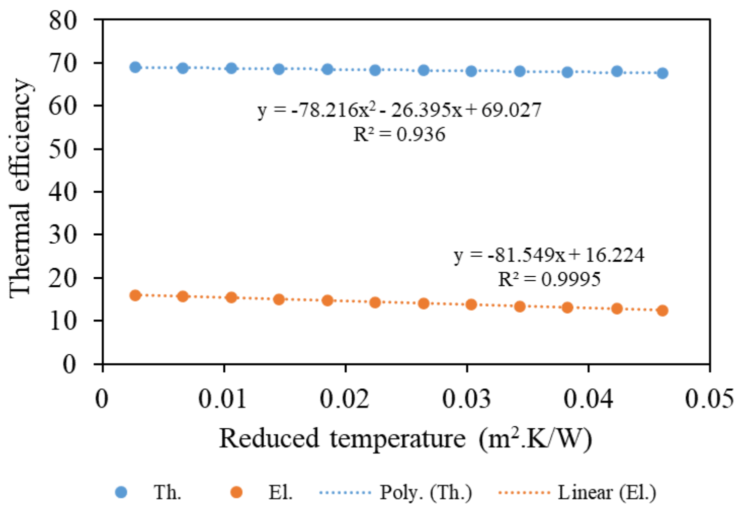

Fig. 6: Characteristic thermal and electrical efficiency curves of the CPV-T collector

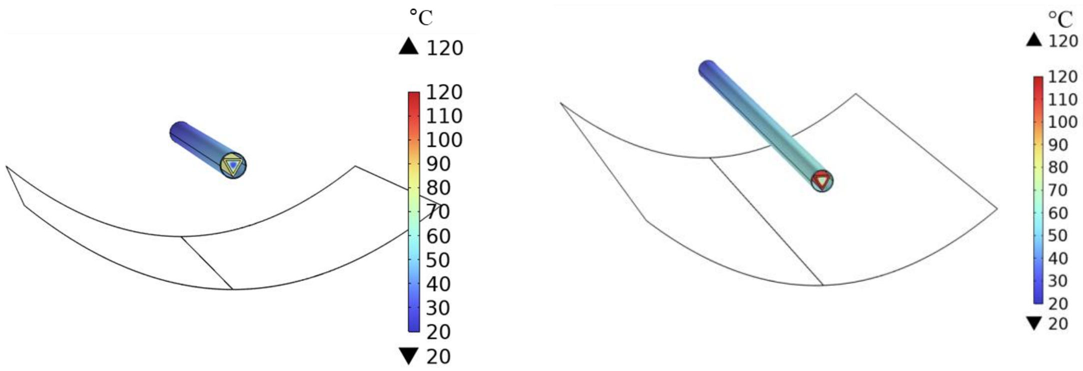

(a) (b)

Fig. 7: Temperature distribution for the CPV-T collector at inlet temperature: (a) 1 °C, and (c) 45 °C

4. Conclusions

A fully coupled optical, electrical and thermal model of a CPV-T collector with a geometrical concentration ratio of 11 was developed. Simulation results revealed that at standard conditions (1000 W/m^2), the total incident power on the aperture of the collector is 3300 W, however, only 2550 W reaches the PV cells, mainly due to optical losses from the mirror and transmission losses from the cover glass. The overall optical efficiency of the collector was 77%. Further, optical simulation results were coupled with a CFD model to estimate the thermal and electrical performance of the collector. Results showed that for an ambient temperature of 25 °C, and an inlet water temperature of 25 °C, the collector can deliver hot water at 77 °C with a thermal efficiency of 68% and an electrical efficiency of 14%. Thereafter, to study the collector's performance in different outdoor conditions, characteristic thermal and electrical efficiency curves as a function of reduced temperature were plotted. The simulations were performed by fixing the heat transfer fluid flowrate and varying its inlet temperature. Results revealed that, the collector can achieve a maximum thermal efficiency of 69% and maximum electrical efficiency of 16%. Based on the investigated design, it is now proposed that passive cooling of the solar cells using spectral splitting will also be explored, while a prototype has been constructed and is being tested in Mexico.

5. Acknowledgments

This work was supported by the UK Engineering and Physical Sciences Research Council (EPSRC) [grant numbers EP/M025012/1, EP/R045518/1, and EP/S032622/1] and an Imperial College London EPSRC Impact Acceleration Account [grant number EP/R511547/1]. The work was also supported by the Royal Society under an International Collaboration Award 2020 [grant number ICA\R1\201302]. The authors would like to thank UK company Solar Flow Ltd. (www.solar-flow.co.uk). Hasan Yildizhan gratefully acknowledges a TÜBİTAK postdoctoral scholarship that supported his visit to Imperial College London. Data supporting this publication can be obtained on request from cep-lab@imperial.ac.uk. For the purpose of Open Access, the authors have applied a CC BY public copyright license to any Author Accepted Manuscript version arising from this submission.

6. References

Acosta-Pazmiño, I. P., Rivera-Solorio, C. I., Gijón-Rivera, M., 2022. Hybridization of a parabolic trough-based thermal plant for industrial heat and power generation. Renewable Energy, 191, 961–973. https://doi.org/10.1016/j.renene.2022.04.074

Barthwal, M., Rakshit, D., 2022. Holistic opto-thermo-electrical analysis of a novel spectral beam splitting-based concentrating photovoltaic thermal system. Journal of Cleaner Production, 379. https://doi.org/10.1016/j.jclepro.2022.134545

Cabral, D., Gomes, J., Hayati, A., Karlsson, B., 2021. Experimental investigation of a CPVT collector coupled with a wedge PVT receiver. Solar Energy, 215, 335–345. https://doi.org/10.1016/j.solener.2020.12.038

Chandan, Baig, H., Tahir, A. ali, Reddy, K. S., Mallick, T. K., Pesala, B., 2022. Performance improvement of a desiccant based cooling system by mitigation of non-uniform illumination on the coupled low concentrating photovoltaic thermal units. Energy Conversion and Management, 257, 115438. https://doi.org/10.1016/j.enconman.2022.115438

Chandan, Dey, S., Iqbal, S. Md., Reddy, K. S., Pesala, B., 2021. Numerical modelling and performance assessment of elongated compound parabolic concentrator based LCPVT system. Renewable Energy, 199–216. https://doi.org/10.1016/j.renene.2020.11.076

Demircan, C., Bayrakçı, H. C., Keçebaş, A., Calise, F., Vicidomini, M., 2023. The effect of temperature distribution on parabolic triangular-based CPVT system performances: Electrical and thermal perspectives. Thermal Science and Engineering Progress, 38, 101664. https://doi.org/10.1016/j.tsep.2023.101664

Deymi-Dashtebayaz, M., Rezapour, M., Farahnak, M., 2022. Modeling of a novel nanofluid-based concentrated photovoltaic thermal system coupled with a heat pump cycle (CPVT-HP). Applied Thermal Engineering, 201, 117765. https://doi.org/10.1016/j.applthermaleng.2021.117765

Herrando, M., Ramos, A., Zabalza, I., Markides, C. N., 2019. A comprehensive assessment of alternative absorber-exchanger designs for hybrid PVT-water collectors. Applied Energy, 235, 1583–1602. https://doi.org/10.1016/j.apenergy.2018.11.024

Hou, Y. tian, Yu, X. hui, Yang, B., Liu, S. shuai, Qi, Y., 2023. Optical performance investigation on flat receiver for parabolic trough solar collector based on the MCRT method. Renewable Energy, 202, 525–536. https://doi.org/10.1016/j.renene.2022.11.109

Huang, G., Markides, C. N., 2021. Spectral-splitting hybrid PV-thermal (PV-T) solar collectors employing semi-transparent solar cells as optical filters. Energy Conversion and Management, 248, 114776. https://doi.org/10.1016/j.enconman.2021.114776

Huang, G., Wang, K., Markides, C. N., 2021. Efficiency limits of concentrating spectral-splitting hybrid photovoltaic-thermal (PV-T) solar collectors and systems. Light: Science and Applications, 10(1), 1–14. https://doi.org/10.1038/s41377-021-00465-1

Karathanassis, I. K., Papanicolaou, E., Belessiotis, V., Bergeles, G. C,. 2017. Design and experimental evaluation of a parabolic-trough concentrating photovoltaic/thermal (CPVT) system with high-efficiency cooling. Renewable Energy, 101, 467–483. https://doi.org/10.1016/j.renene.2016.09.013

Liang, H., Su, R., Huang, W., Cheng, Z., Wang, F., Huang, G., Yang, D., 2022. A novel spectral beam splitting photovoltaic/thermal hybrid system based on semi-transparent solar cell with serrated groove structure for co-generation of electricity and high-grade thermal energy. Energy Conversion and Management, 252, 115049. https://doi.org/10.1016/j.enconman.2021.115049

Madurai Elavarasan, R., Mudgal, V., Selvamanohar, L., Wang, K., Huang, G., Shafiullah, G. M., Markides, C. N., Reddy, K. S., Nadarajah, M., 2022. Pathways toward high-efficiency solar photovoltaic thermal management for electrical, thermal and combined generation applications: A critical review. Energy Conversion and Management, 255, 115278. https://doi.org/10.1016/j.enconman.2022.115278

Parthiban, A., Mallick, T. K., & Reddy, K. S., 2022. Integrated optical-thermal-electrical modeling of compound parabolic concentrator based photovoltaic-thermal system. Energy Conversion and Management, 251, 115009. https://doi.org/10.1016/j.enconman.2021.115009

Yousef, M. S., Abdel Rahman, A. K., Ookawara, S., 2016. Performance investigation of low – Concentration photovoltaic systems under hot and arid conditions: Experimental and numerical results. Energy Conversion and Management, 128, 82–94. https://doi.org/10.1016/j.enconman.2016.09.061

Appendix: Units and Symbols

Table 2: List of symbols

Quantity	Symbol	Unit
Absorptance	α	
Acceleration due to gravity	g	m/s^2
Aperture area	A_{ap}	m^2
Density	ρ	kg/m^3
Dynamic viscocity	μ	Pa.s
Efficiency	η	%
Emittance	ε	
Mass flowrate	$\dot{m}$	kg/s
Pressure	P	Pa
Reduced temperature	T_r	K.m^2/ W
Reflectance	r	
Shear stress	τ	Pa
Specific heat	c_p	J/ (kg.K)
Temperature	T	K
Temperature coefficienct of power	β	% /K
Thermal conductivity	k	W/(m.K)
Transmittance	τ	
Velocity	v	m/s

Table 3: List of subscripts

Quantity	Symbol
Reflection	ref
Incident	inc
Photovoltaic	pv
Thermal	th
Outlet fluid	fo
Inlet fluid	fi
Aperture	ap
Ambient	amb